A. I.

# ADIABATIC SHEAR-BANDING IN HIGH-STRENGTH ALLOYS

John H. Beatty †
Yeou-Fong Li ††
Marc A. Meyers ††
Sia Nemat-Nasser ††

† US Army Materials Technology Laboratory, Watertown MA 02172
†† University of California-San Diego, La Jolla CA 92093

## ABSTRACT

A special experimental technique has been developed by which adiabatic shear bands can be generated under controlled conditions to allow for an experimental and theoretical study of adiabatic shear-banding in high-strength alloys. This allows the systematic examination of the shear-band microstructure at various stages of its evolution. The technique has been used to develop shear bands in AISI 4340 steel for a variety of quenched and tempered microstructures. Both the strain and strain rate were controlled. The shear-band microstructure has been analyzed using optical, scanning electron, and transmission electron microscopy. Parallel with this work, Hopkinson bar techniques were used to develop high-strain, high-strain-rate constitutive properties of the material. These properties were then embedded in a viscoplastic constitutive model and used in the explicit finite element computer code PRONTO 2D to study the deformation of the specimen, leading to initiation and growth of shear bands.

This paper presents observations of the microstructure of shear bands, results of the high-strain, high-strain-rate constitutive relations of the material used, and a set of finite-element simulations of the experiment.

## INTRODUCTION

During high-strain-rate deformation, a localized region (the shear band) is sheared at a sufficiently high strain rate to preclude significant heat transfer away from the deforming zone. Many processes such as turning, reaming, punching, projectile deformation, and armor penetration can create adiabatic shear bands in a variety of ductile materials. Material within the band undergoes both a large accumulated strain and a significant increase in temperature.

This study aimed at developing a thorough understanding of microstructural influences on shear-band initiation. "Hat"-shaped specimens were tested using a split-Hopkinson compression bar (following Meyer [1,2]). Previously, we tested several microstructures of a VAR 4340 steel to compare resistance to shear-band formation. These preliminary results showed the technique was sensitive to microstructural changes and allowed for metallographic examination of the band at various stages of its formation[3]. Thus this "hat" test has proved very useful for qualitative comparisons.

To complement the microstructural study, the hat test itself has been examined using a phenomenological viscoplastic constitutive model. The high-strain-rate properties are determined by a series of standard split Hopkinson compression tests at different strain rates. These relations are then used in the explicit finite-element code PRONTO 2D to study the deformation of the specimen and the initiation and growth of the shear bands. Thus we have simultaneously examined both the hat test as well as the predictive capabilities of the model itself.

## EXPERIMENTAL PROCEDURE

A VAR 4340 steel alloy was used in the current study. Four microstructures were examined, all of which have a hardness of Rockwell C 52. The size and distribution of the grain-refining carbides was varied by using a two-step austenitizing treatment. The first austenitization was carried out at either 845°C, 925°C, 1010°C, or 1090°C for two hours. At each austenitizing temperature, a unique distribution of grain-refining carbides is produced by the differences in dissolution and/or coarsening rates. The second short austenitizing treatment at 845°C for 15 minutes was too short to significantly alter the carbide distribution, but restored a uniform

austenite grain size. These microstructures have been previously characterized by Cowie [4,5] and examined in our earlier paper[3].

The specimen configuration used is shown in Figure 1. Under uniaxial compression, the hat-shaped, cylindrically symmetric specimen undergoes intense shearing in the regions indicated in the side cutaway portion of the figure. To limit this shear deformation, precision machined "stop rings" are placed around the upper portion of the hat, to halt the shearing process at selected stages of shear-band formation. From these interrupted samples, metallographic, SEM, and TEM specimens are produced to observe microstructure-deformation interactions.

The samples are loaded in compression using a compression split-Hopkinson bar. The profile of the compression pulse impinging on the sample through the incident bar is controlled by placing a copper cushion at the striker end of the incident(input) bar; see Nemat- Nasser [6] for details.

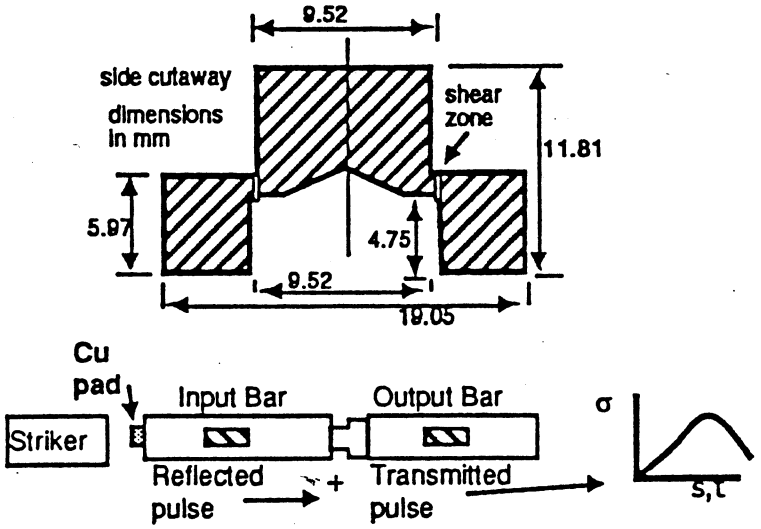


Figure 1. Hat specimen dimensions and split Hopkinson apparatus.

TEM samples of the sheared regions were made by mechanically thinning the material to a thickness of less than 0.125mm. Discs 3 mm in diameter were abrasively cut from the thinned material using a slurry disc cutter. The foils were electropolished in a 5% perchloric 95% methanol solution at -20°C and 50 volts. The shear-band region polished preferentially, but produced insufficient electron transparent regions. Ion milling at 15 degrees impact angle and 4 kV was used to further thin the specimens for TEM

examination. Both a 300kV Philips CM-30 and a JEOL 200 CX electron microscope were used.

## NUMERICAL SIMULATION

Quasi-static and high-strain-rate simple compression tests were performed on samples of a single microstructure (austenitized at 845°C). The results were used for constitutive modelling and were subsequently integrated into the finite-element simulation of the hat-shaped tests. For this purpose, strain rates from $8 \times 10^{-4}$ to $4 \times 10^{3}$ / s were used.

An elastoviscoplastic constitutive model is used, in which the deviatoric deformation rate tensor $\underset{\sim}{D}'$ is decomposed into an elastic and a viscoplastic part,

$$\underset{\sim}{D}' = \underset{\sim}{D}'^{el} + \underset{\sim}{D}'^{pl} \tag{1}$$

where

$$\underset{\sim}{D}'^{el} = \frac{1}{2G}\overset{\circ}{\underset{\sim}{\tau}}' \quad , \tag{2}$$

$$\underset{\sim}{D}'^{pl} = \dot{\gamma}\frac{\underset{\sim}{\tau}'}{\sqrt{2}\tau}, \quad \tau = \sqrt{\frac{1}{2}\underset{\sim}{\tau}':\underset{\sim}{\tau}'} \quad . \tag{3,4}$$

Above, $\underset{\sim}{\tau}'$ is the deviatoric portion of the Cauchy stress, and $\overset{\circ}{\underset{\sim}{\tau}}'$ is an objective stress rate; in the computer code PRONTO 2D[7], the stress rate is calculated in the Lagrangian triad and hence, the objective stress rate is defined, using the spin of the Eulerian triad relative to the Lagrangian triad; see Nemat-Nasser[8].

In the elastoviscoplastic model used here, the plastic shear strain rate, $\dot{\gamma}$, is assumed to relate to the rate-dependent flow stress in shear of the material, $\tau_y$, in the following manner:

$$\tau_y = \tau_o\left(\frac{\dot{\gamma}}{\dot{\gamma}_o}\right)^{\left(\frac{1}{m}\right)}\left(1+\frac{\gamma}{\gamma_o}\right)^{N} e^{-\lambda(\Delta T)} \quad , \tag{5}$$

where $\tau_0$ and $\gamma_0$ are the initial flow stress and flow strain, respectively, at some reference strain rate $\dot{\gamma}_o$, and N, m, and $\lambda$ are material parameters. In eqn. (5),

$$\Delta T = \int_0^t \chi\xi\tau\dot{\gamma}dt \quad , \quad 0<\chi\leq 1 \quad , \tag{6}$$

where $\chi$ represents the fraction of plastic work which is converted to heat, and $\xi$ is a dimensional parameter which relates the rate of plastic work to the change in the temperature, $\Delta T$, of the material; $\xi = 2.7455 \times 10^{-7} m^3 °C/J$, for this case.

To fix the material parameters N and m, as well as the reference quantities $\tau_o$ and $\gamma_o$, simple quasi-static and Hopkinson bar compression tests were used. For the quasi-static experiments, the temperature effects in (5) can be neglected. At increasing strain-rates, however, some of the heat generated remains within the deforming sample, causing thermal softening. For our final simulation of the hat specimen, the plastic deformation was localized over a very small region, and since the test duration was suitably short, one can assume the process was completely adiabatic with good accuracy. Therefore, we first determined $\tau_o$, $\gamma_o$, m, and N, using a least-squares scheme. This produced $\tau_o = 1030$ MPa ($\sigma_{o\ eff} = 1790$ MPa), $\gamma_o = 0.015$, m = 90, and N = 0.0875. For different strain rates the parameters $\lambda$ and $\chi$ change, and had to be fitted to the experimental data. A simple procedure is to set $\lambda$ equal to a constant, and then change $\chi$ for different strain rates. For example, we obtained $\lambda = 0.0019$ and $\chi = 1.0, 0.8, 0.72$ for strain rates of 4000, 2000, and 1200 $sec^{-1}$, respectively. Figure 2 shows the true

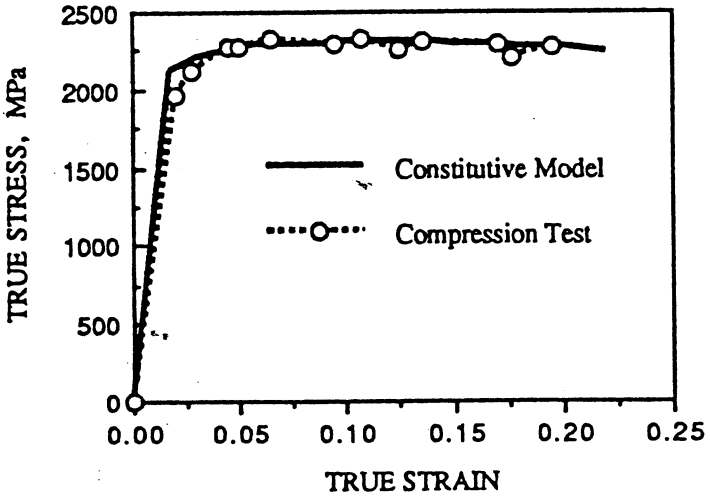


Figure 2. True stress vs. true strain curve from constitutive model and experimental data (o) from split Hopkinson compression tests. $\dot{\varepsilon}$ = 2000/s.

stress vs. true strain obtained in this manner for a strain rate of 2000 $sec^{-1}$, along with the experimental data. Similar good fits were achieved for the other strain rates. For the adiabatic case, $\chi = 1$.

## EXPERIMENTAL RESULTS AND DISCUSSION

From the stress-time and velocity-time curves obtained during the hat test, a stress displacement plot is generated by integrating the velocity-time curve. A typical shear stress vs. displacement curve for this steel is shown in Figure 3. For these microstructures, the samples showed a large linear region, and the stresses fell smoothly after instability. Instability is defined as the point where the shear stress reaches its maximum value. The shear strain rate is estimated from combining the measured width of the deforming zone (from optical cross sections prior to shear-band formation) and the displacement rate, giving $\dot{\gamma} \approx 1.01 \times 10^5 s^{-1}$. This shear strain rate and resulting strain are not entirely uniform, as the geometry of the sample creates some localization at the outset of the test.

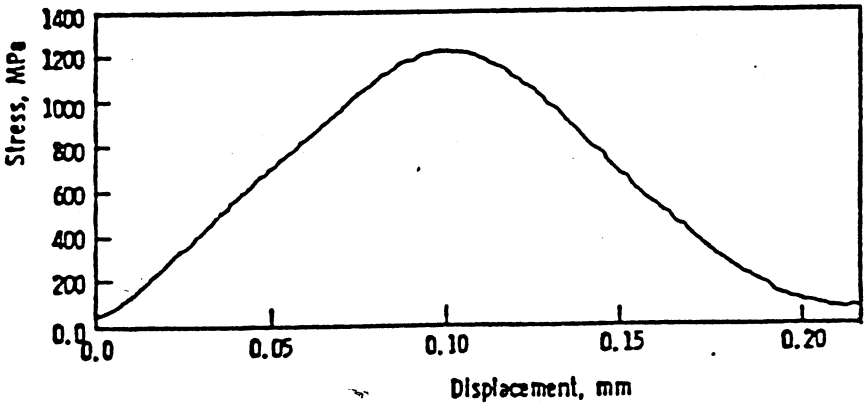


Figure 3. Typical shear stress-displacement curve of VAR4340 steel at a hardness of Rc52. This sample was given its first austenitization treatment at 1090°C.

Figure 4 shows shear band development using optical(4a) and scanning electron microscopy(4b,c) in typical samples. The shear bands etch white in nital, typical of the so-called "transformed" band type. Figure 4b,c are SEM micrographs of a shear band formed in the microstructure normalized at 925°C. Figure 4c shows this band near its tip. Note the alignment of the martensite laths with the shearing direction along the band edges and the absence of any resolvable grain structure within the band at this magnification.

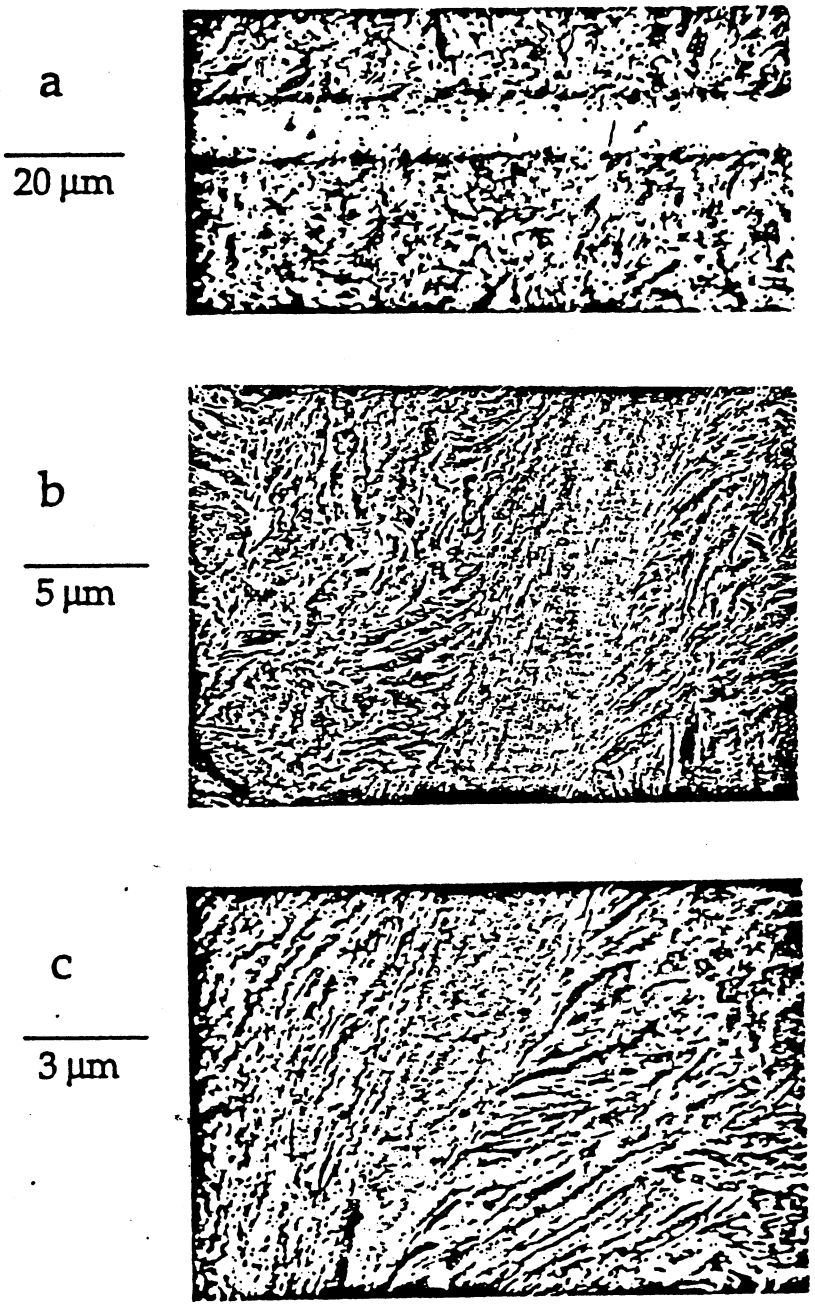


Figure 4. Micrographs of shear bands produced using the "hat" specimen developed by Meyer[1,2]. a) Optical micrograph of the shear band. b) Scanning electron micrograph showing lath realignment and "flow" regions near the edge of the band. c) Propagating shear band at the tip.

"Flow" lines (martensite lath realignment) can be detected parallel to the shear direction within the band.

The maximum shear stress attained was virtually independent of the four microstructures tested. The same microstructures were previously studied[4,5] at low strain rates in pure shear, and here too, no effect on the instability stress was found. However, significant differences between the microstructures were noted when energy absorption was considered. Figure 5 plots the energy absorbed before instability ($E_i$) vs. austenitizing temperature relationship for a strain rate of $\dot{\gamma} \approx 10^5 s^{-1}$; note the energy peak for the 925°C austenitizing temperature. Recent work also suggests that resistance to ballistic failure by plugging in thin plate follows the same trend[9].

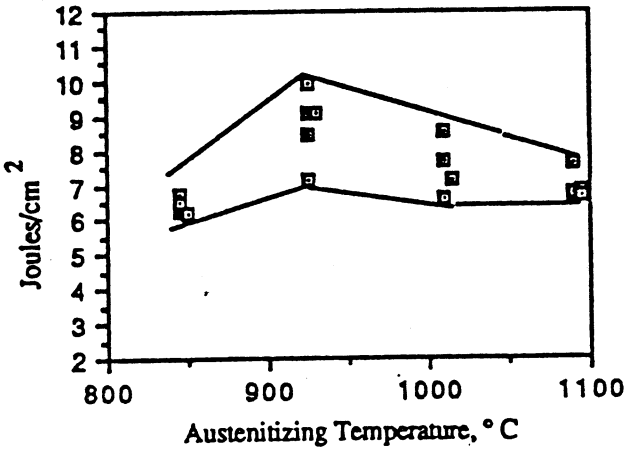


Figure 5. Energy absorbed to the point of instability per unit area sheared, Ei, versus austenitizing temperature.

Dark-field transmission electron microscopy was used to examine a region near the center of the shear band. By centering the first bright ring along the optical axis, the microcrystals can be individually illuminated. Figure 6 is such a dark-field micrograph where the crystallite size can be determined to range from 8 to 20nm. This size is an order of magnitude smaller than previously assumed[10], but otherwise the structure is in general agreement with earlier TEM evaluations of shear bands[3,10-14]. The change from a true microcrystalline structure to "normal" heavily deformed martensite away from the band was gradual, as verified previously[3] using Selected Area Diffraction Patterns (SADPs) as a function of distance away from the center of the band.

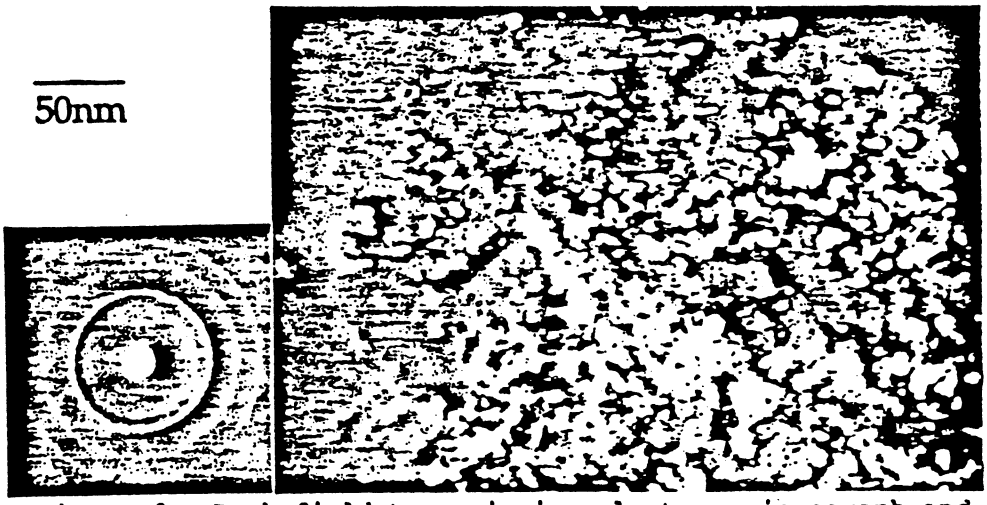


Figure 6. Dark-field transmission electron micrograph and selected area diffraction pattern taken from the center of a shear band. Microcrystals range from 8 to 20nm in diameter.

No carbide spots or austenite reflections could be found near the center of the band. The extremely fine grain size and rapid quench rate should increase levels of retained austenite, if any martensite transformed while shearing. The absence of any austenite reflection near the center of the band therefore suggests that no transformation has occurred for this particular case, and that the increased hardness and white etching characteristics are caused by the ultra-fine grain size and the breakup/dissolution of carbides.

## NUMERICAL SIMULATION RESULTS

The results from the finite-element calculations are given in Figures 7-10. Figure 7 shows the undeformed and deformed meshes. The initial transverse element width in the concentrated shear region is 18 μm, which compares to the observed shear band width of 9-15 μm in the microstructures studied (compare to Figure 4a). The intense shearing occurs within one single column of elements, which shows that shear band width will vary with choice of element size, no matter how small of a mesh size is selected. Previously Olson, Mescall and Azrin demonstrated this limitation[15], but it is not within the scope of this work to address this important problem. The total shear strain profile from point A

a)

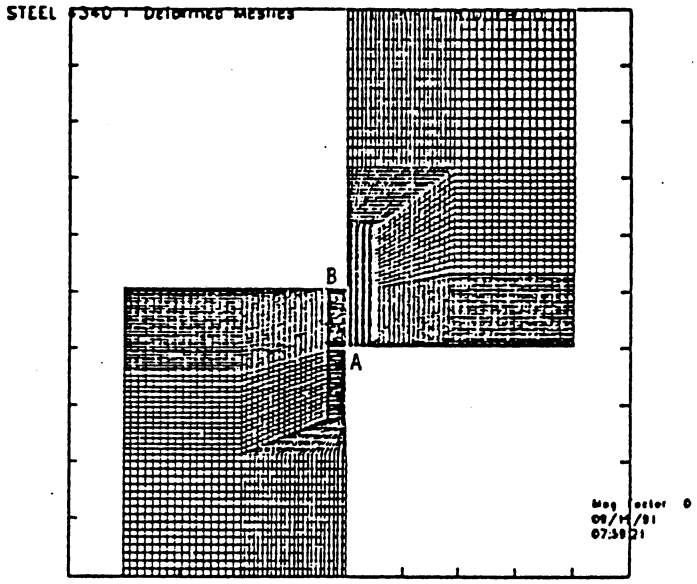


b)

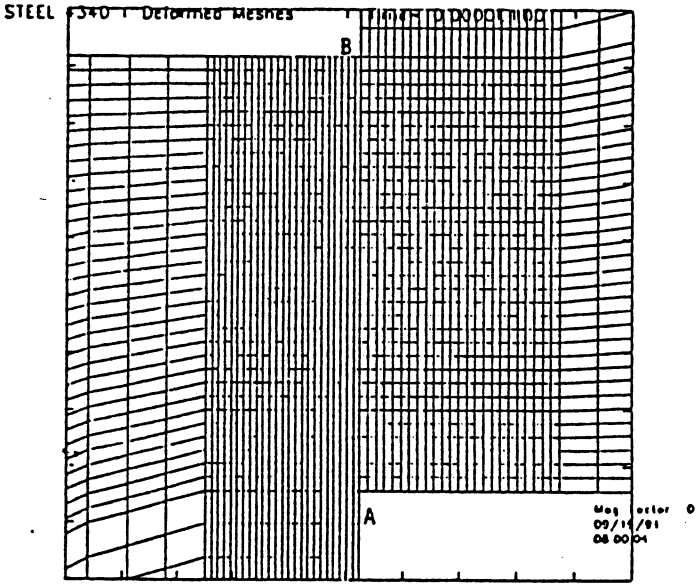


Figure 7. Finite-element meshes. Undeformed finite- element meshes used to simulate the hat test. a) Entire specimen. b) Concentrated shear region. Width of elements is 18 μm in the shear zone.

c)

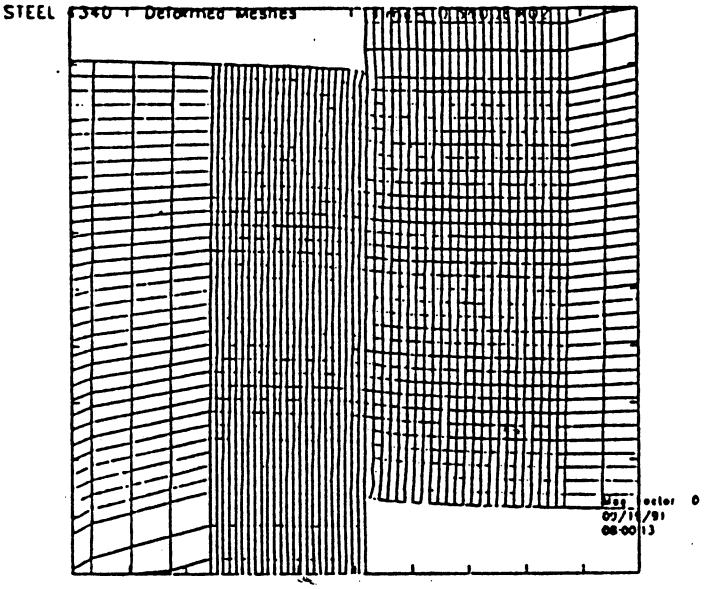


d)

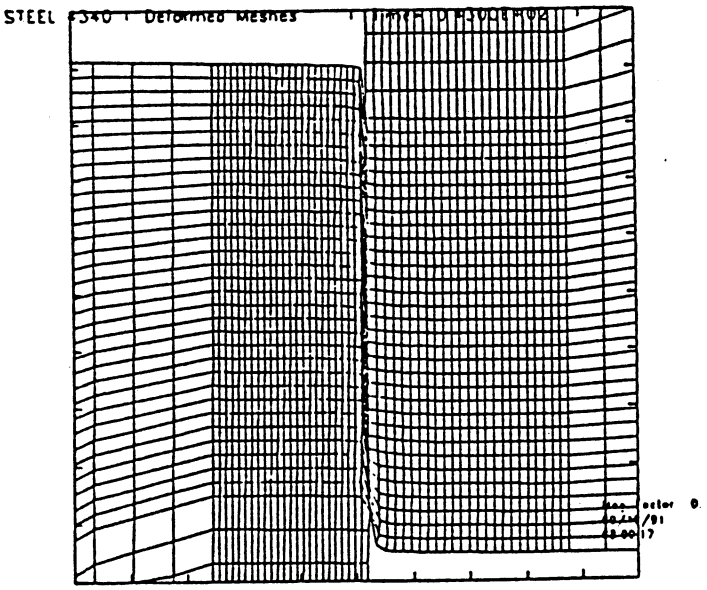


Figure 7, continued. c) Deformed mesh at the instability point (33μsecs). d) Deformed mesh at end of simulation (43μsecs).

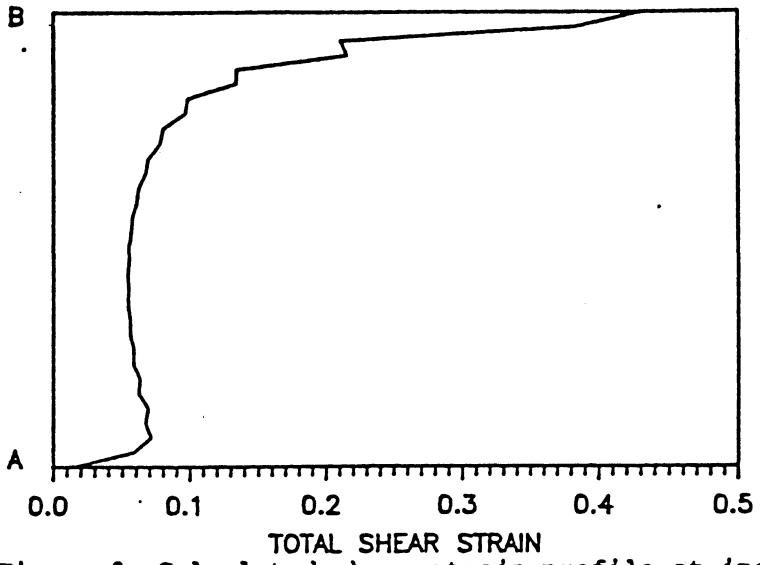


Figure 8. Calculated shear strain profile at instability. (A-B as denoted in Figure 7.)

to point B (see Figure 7) calculated at the instability point is given in Figure 8. Shear strains range from about 0.1 in much of the band to 0.45 near point B.

Of further interest is the temperature range predicted near the point of instability. Figure 9 gives the predicted temperature profile from point A to point B in the concentrated shear region, just before thermal instability is reached. The temperatures predicted just before instability, at 34 μsecs, are fairly low, with the highest temperature reaching only 160°C at point B. Just after instability, at 35μsecs, the predicted profiles suddenly jump to extremely high levels - above 2000°C- and we do not consider the solution to be valid close to this state (Figure 10). Though the model does predict thermal destabilization near the appropriate point of the stress-time curve, the degree of destabilization predicted is too great, and is largely dependent on the value of $\lambda$ in eqn(5); clearly, $\lambda$ cannot remain constant over such broad ranges of strain rates and temperatures. Further work is needed to adapt the constitutive model to work in this extreme regime of high-temperature, large-strain, and high-strain-rate deformation, where the shear band may be regarded as a discontinuity.

The simulation also produces stress-time curves, analogous to the data obtained in the split Hopkinson hat test. Therefore we can compare the experimental results from the hat test to the model predictions. This comparison is shown in Figure 11. Thus, the

finite-element model based on constitutive relations derived from simple compression tests gives reasonable results when used to predict a much more complex experiment, at least to the point of destabilization. Although some potentially important aspects are ignored (for example, the effect of confining pressure), the simulation does closely reproduce the observed experimental behavior. This suggests that equations of the form of equation (5) can be used in a variety of complex high-strain, high-strain-rate approximations after the parameters are fitted to a series of simpler high-strain-rate tests.

## CONCLUSIONS

The hat specimen technique utilized in this study allows for the systematic examination of shear band microstructures at various stages of its evolution, and gives a qualitative comparison of shear band initiation resistance. A constitutive model and finite-element simulation based on simpler compression tests at various strain rates is in good agreement with the experiment up to and including the onset of thermal destabilization. However, the degree of destabilization predicted by the simulation is too extreme because of the assumed constant value of the parameter $\lambda$. Further refinement of the constitutive model is possible through a more realistic representation of the thermal softening effect.

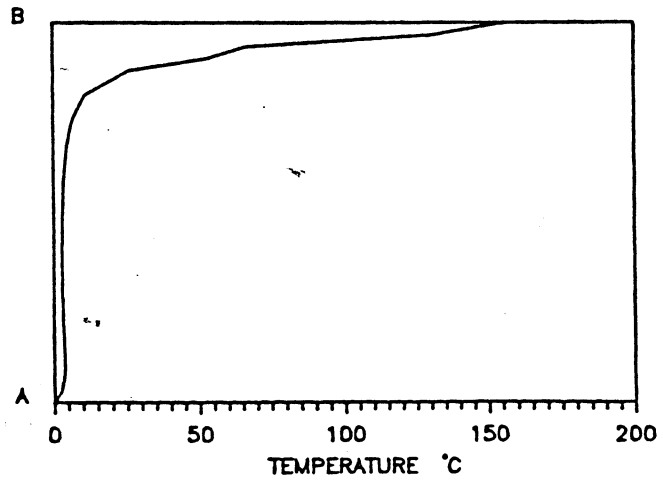


Figure 9. Simulated temperature profile of shear region at 34μsecs, just before instability (A-B as in Figure 7).

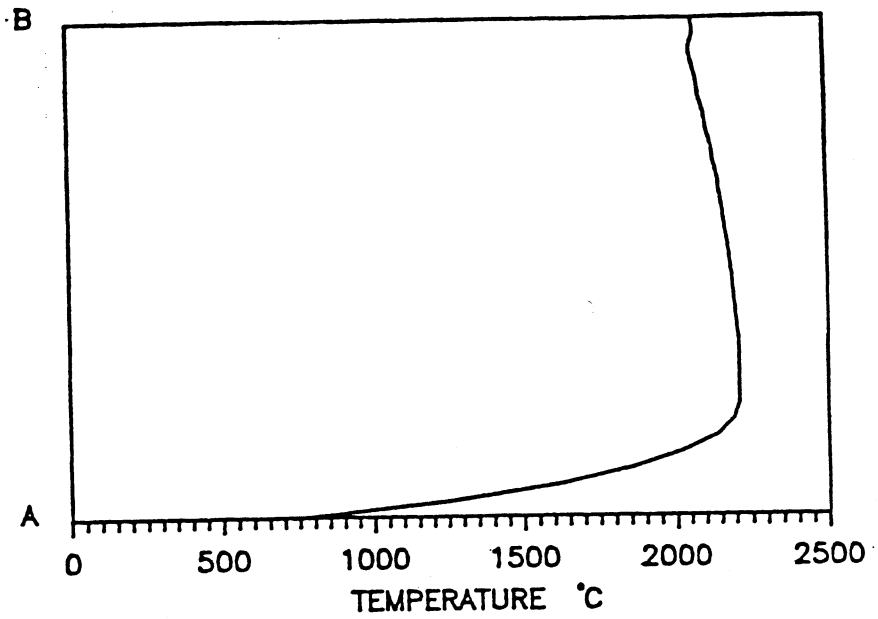


Figure 10. Simulated temperature profile of the concentrated shear region at 35μsecs, after instability. The solution is of questionable validity for this state (A-B as in Figure 7).

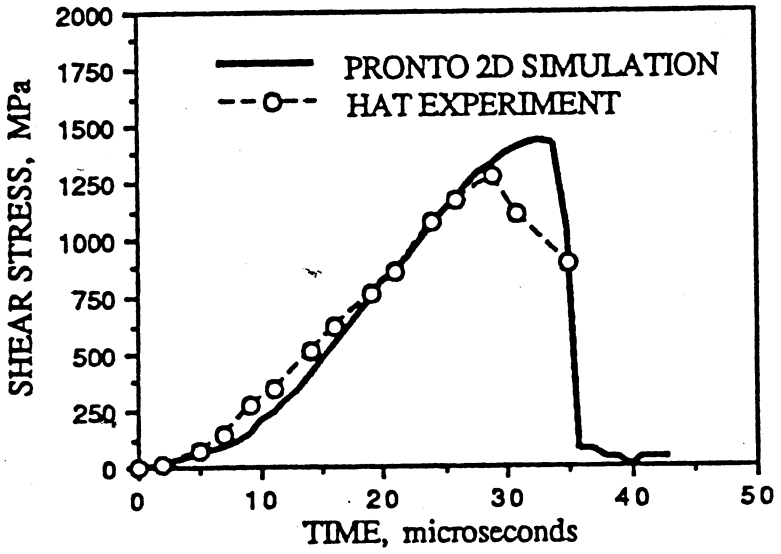


Figure 11. Stress-time curves. 1) Predicted by the finite-element model (solid line) and 2) Measured during the hat test (open circles).

REFERENCES


1. K-H Hartman, H.D. Kunze, and L.W. Meyer, "Metallurgical Effects on Impact Loaded Materials," in Shock Waves and High-Strain-Rate Phenomena in Metals, M.A. Meyers and L.E. Murr, eds, pub Plenum Press, New York, 1981.

2. L.W. Meyer, and S. Manwaring, "Critical Adiabatic Shear Strength of Low Alloyed Steel Under Compressive Loading,"in Metallurgical Applications of Shock-Wave and High-Strain-Rate Phenomena, L.E. Murr, K.P. Staudhammer, and M.A. Meyers, eds., pub Marcel Dekker, Inc, New York,1986.

3. J.H. Beatty, L.W. Meyer, M.A. Meyers, and S. Nemat-Nasser, "Formation of Controlled Adiabatic Shear Bands in AISI 4340 High Strength Steels," in Shock Waves and High Strain-Rate Phenomena in Materials, eds. Meyers, Murr, Staudhammer, published by Marcel Dekker, 1991.

4. J.G. Cowie, "The Influence of Second Phase Dispersions on Shear Instability and Fracture Toughness of Ultrahigh Strength 4340 Steel," US Government Report MTL TR 89-20, March 1989.

5. M. Azrin, J.G. Cowie, and G.B. Olson, "Shear Instability Mechanisms in High Hardness Steel," US Government Report MTL-TR 87-2, January 1987.

6. S. Nemat-Nasser, J.B. Issacs, and J.E. Starrett, "Hopkinson Techniques for Dynamic Recovery Experiments," Technical report of the University of California, San Diego, Center of Excellence for Adv. Materials, Feb. 1991.

7. L.M. Taylor and D.P. Flanagan, "PRONTO 2D: A Two-Dimensional Transient Solid Dynamics Program," Sandia Report, SAND86-0594, 1987.

8. S. Nemat-Nasser, "Certain Basic Issues in Finite-Deformation Continuum Plasticity," *Mechanica*, 25, p.223-229 , 1990.

9. J.H. Beatty and M. Azrin , 1991 (to be published).

10. Y. Meunier, L. Sangoy, and G. Pont, "Metallurgical Aspects of Adiabatic Shear Phenomenon in Armor Steels with Perforation," in Impact Loading and Dynamic Behaviour of Materials, C.Y. Chiem, H.-D. Kunze, L.W. Meyer, eds, DGM Informations gesellschatt, Oberursel/Frankfurt, Vol 2:711, 1988.

11. R.C. Glenn and W.C. Leslie, Met Trans 1971 v2, p2954.

12. A.L. Wingrove," A Note on the Structure of Adiabatic Shear Bands in Steel", Australian Defense Standard Laboratories, Technical Memo., 33 1971.

13. C.L. Wittman and M.A. Meyers, "Effects of Metallurgical Parameters on Shear Band Formation in a Low Carbon Steels," submitted to Metall. Trans.

14. C.L. Wittman, M.A. Meyers, and H.-r Pak, "Observation of an Adiabatic Shear Band in AISI 4340 Steel by High Voltage Electron Microscopy," Metall. Trans., V 21 A, March 1990.

15. G.B. Olson, J.F. Mescall, and M. Azrin, "Adiabatic Deformation and Strain Localization'" in Shock Waves and High-Strain-Rate Phenomena in Metals, eds. Meyers, Murr, pub. Plenum, 1981.